Electronic Supplementary Material (ESI) for Dalton Transactions.

Supporting Information

Constructing High Axiality Mononuclear Dysprosium Molecular Magnets by Regulating the Co-ligands Strategy

Jia-Ling Wang, [a] Ji-Tun Chen, [a] Han Yan, [a] Tian-Tian Wang, [a] Yi-Quan Zhang *[b] and Wen-Bin Sun *[a]

[a] Key Laboratory of Functional Inorganic Material Chemistry Ministry of Education, School of Chemistry and Material Science Heilongjiang University, 74 Xuefu Road, Harbin 150080, P. R. China. *E-mail: wenbinsun@126.com*

[b] Jiangsu Key Laboratory for NSLSCS, School of Physical Science and Technology, Nanjing Normal University, Nanjing 210023, P. R. China. *E-mail: zhangyiquan@njnu.edu.cn*

Table S1. Crystallographic data for complexes **1** and **2**.

	1	**2**
Empirical formula	$C_{34}H_{25}DyF_{15}N_5O_3$	$C_{52}H_{51}BDyF_4N_5O_2$
Formula weight	999.09	1027.28
Crystal system	monoclinic	orthorhombic
Space group	I2/a	$P2_12_12_1$
Temperature (K)	293(2)	293.0
a (Å)	22.4801(12)	10.2351(6)
b (Å)	10.6886(6)	17.8266(13)
c (Å)	30.427(2)	27.2325(16)
α (°)	90	90
β (°)	96.817(5)	90
γ (°)	90	90
V (Å^3)	7259.4(7)	4968.8(5)
ρ_{calc} (Mg m^{-3})	1.828	1.373
μ (mm^{-1})	2.179	8.526
F(000)	3912.0	2084.0
Collected reflections	22269	9071
Independent reflections	6405	9071
*R*int	0.0550	0.0037
R_1 [$I > 2\sigma(I)$]	0.0581	0.0755
wR_2 (all data)	0.1031	0.2308
Goodness of fit on F^2	1.119	1.062
CCDC number	2300916	2300917

Table S2. Selected bond lengths (Å) and angles (°) for complex **1**.

Dy1-O1	2.229(5)	O2-Dy1-O3	138.62(19)
Dy1-O2	2.285(5)	O1-Dy1-N1	73.6(2)
Dy1-O3	2.294(5)	O1-Dy1-N2	89.6(2)
Dy1-N1	2.447(6)	O1-Dy1-N3	126.6(3)
Dy1-N2	2.456(7)	O1-Dy1-N4	121.3(3)
Dy1-N3	2.538(8)	O1-Dy1-N5	80.6(2)
Dy1-N4	2.455(7)	O2-Dy1-N1	146.59(19)
Dy1-N5	2.456(8)	O2-Dy1-N2	111.2(2)
O1-Dy1-O2	73.25(19)	O2-Dy1-N3	71.5(3)
O1-Dy1-O3	148.0(2)	O2-Dy1-N4	73.2(3)
O2-Dy1-N5	113.9(2)	N1-Dy1-N4	129.7(3)
O3-Dy1-N1	74.7(2)	N1-Dy1-N5	64.4(3)
O3-Dy1-N2	80.8(2)	N2-Dy1-N3	68.0(3)
O3-Dy1-N3	77.8(3)	N2-Dy1-N4	147.7(3)
O3-Dy1-N4	76.9(3)	N2-Dy1-N5	128.4(3)
O3-Dy1-N5	81.7(2)	N4-Dy1-N3	84.4(3)

N1-Dy1-N2	64.2(2)	N5-Dy1-N3	151.0(3)
N1-Dy1-N3	127.7(3)	N5-Dy1-N4	71.1(3)

Table S3. Selected bond lengths (Å) and angles (°) for complex **2**.

Dy1-O1	2.156(11)	O2-Dy1-N1	95.1(5)
Dy1-O2	2.160(10)	O2-Dy1-N2	90.9(5)
Dy1-N1	2.404(11)	O2-Dy1-N3	87.5(6)
Dy1- N2	2.500(2)	O2-Dy1-N4	86.2(6)
Dy1- N3	2.450(19)	O2-Dy1-N5	92.5(5)
Dy1-N4	2.480(2)	N1-Dy1-N2	65.3(6)
Dy1-N5	2.351(19)	N1-Dy1-N3	136.9(6)
Dy2-N6	2.505(7)	N1-Dy1-N4	138.4(6)
Dy2-N3	2.498(7)	N3-Dy1-N2	71.7(7)
O1-Dy1-O2	168.5(19)	N3-Dy1-N4	84.6(7)
O1-Dy1-N1	95. 5(5)	N4-Dy1-N2	156.2(6)
O1-Dy1-N2	89.5(6)	N5-Dy1-N1	67.2(6)
O1-Dy1-N3	81.7(6)	N5-Dy1-N2	132.5(7)
O1-Dy1-N4	88.9(6)	N5-Dy1-N3	155.8(7)
O1-Dy1-N5	95.7(5)	N5-Dy1-N4	71.2(7)

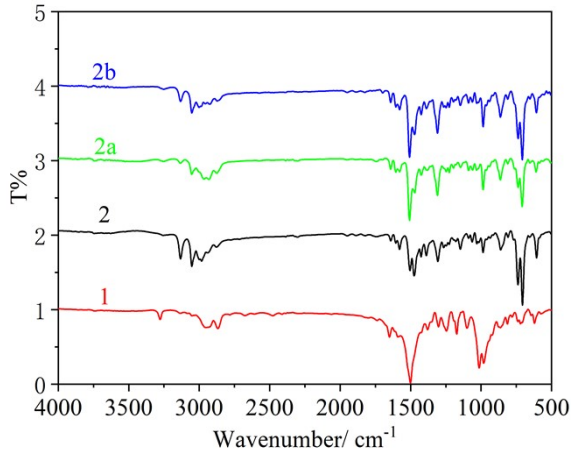

Fig. S1 Infrared spectra for **1**, **2**, **2a** and **2b**.

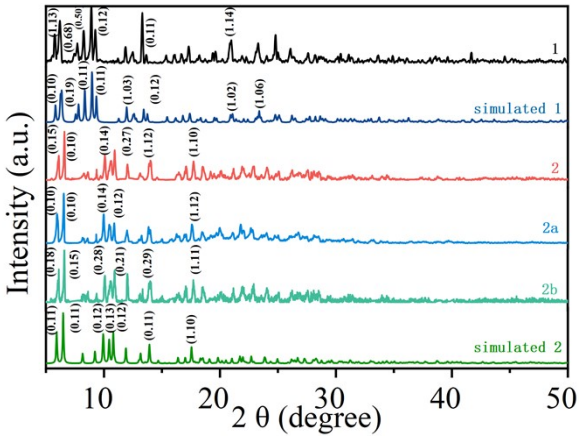

Fig. S2 Experimental and simulated X-ray powder diffraction patterns for **1, 2, 2a** and **2b** (The simulation

model is exported from Mercury using CIF file).

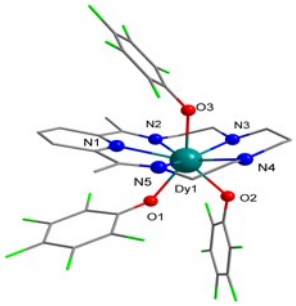

Fig. S3 Structure of complex **1**

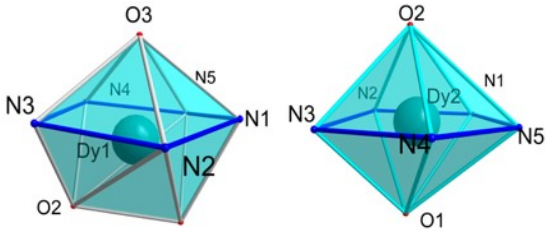

Fig. S4 Coordination polyhedra for complex **1** and **2**

Table S4. Continuous Shape Measures (CShMs) of the coordination geometry for Dy^{III} ion in complex **1** (CShMs values calculated with the Shape program). The CShMs values indicated the proximity to the ideal polyhedron, thus, CShMs = 0 corresponds to the non-distorted polyhedron. The three closer ideal geometries to the real complexes are listed and below are the symmetry and description for each polyhedron.

	CShMs	Polyhedron		
1	2.138	TDD-8	D_{2d}	Triangular dodecahedron
	4.625	SAPR-8	D_{4d}	Square antiprism
	8.484	CU-8	O_h	Cube
2	1.207	PBPY-7	D_{5h}	Pentagonal bipyramid
	2.785	JPBPY-7	D_{5h}	Johnson pentagonal bipyramid J13
	5.765	CTPR-7	C_{2v}	Capped trigonal prism

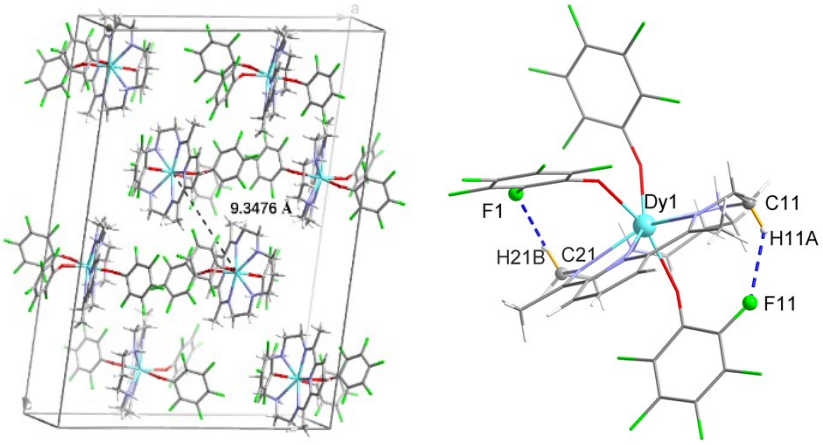

Fig. S5 The packing diagram for complex **1** gives the shortest Dy···Dy distance of 9.3476 Å and the possible

intramolecular C-H···F interactions.

Table S5. C-H···F bond lengths (Å) and angles (°) for complexes **1**.

Complex **1**

D-H-A	d(D-H)/Å	d(H-A)/Å	d(D-A)/Å	D-H-A/°
C11-H11···F11	0.970	2.597	3.347	134.350
C21-H21···F1	0.970	2.592	3.256	125.772

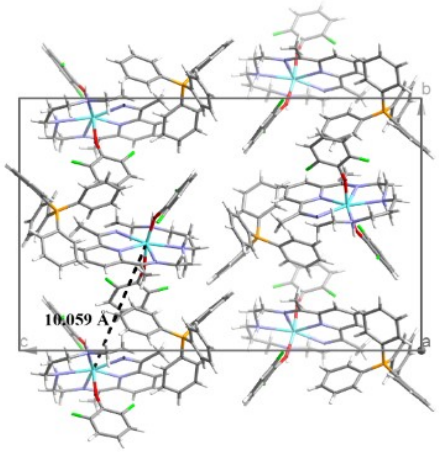

Fig. S6 The packing diagram for complex **2** gives the shortest Dy···Dy distance of 10.059 Å.

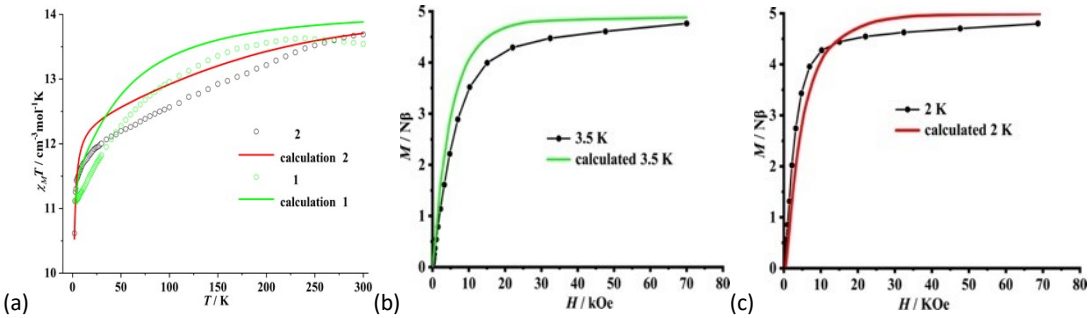

Fig. S7 (a) Temperature dependence of the magnetic susceptibility χ_MT at 1000 Oe for complexes **1** (green circle) and **2** (black circle), calculated magnetic susceptibilities of complexes **1** (green solid line) and **2** (red solid line) (b) calculated magnetization curves for **1** at 3.5 K, (c) calculated magnetization curves for **2** at 2 K. using CASSCF/RASSI-SO with OpenMolcas.

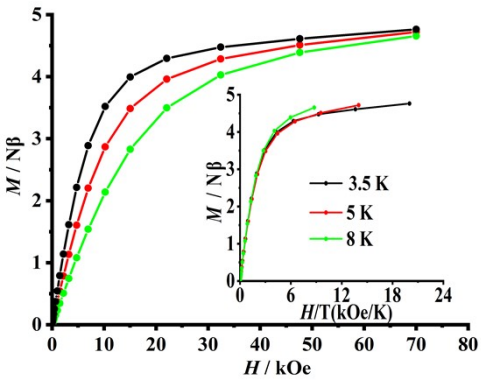

Fig. S8 Field dependences of magnetization in the field range 0–70 kOe and temperature range 3.5–8 K for **1**

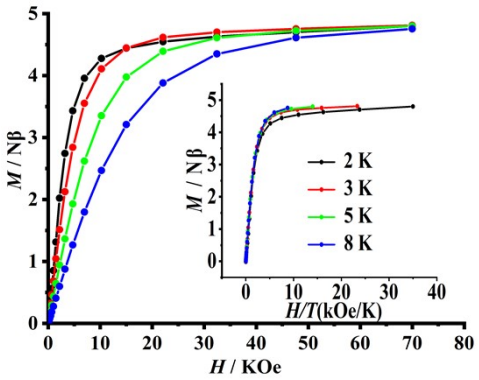

Fig. S9 Field dependences of magnetization in the field range 0–70 kOe and temperature range 2–8 K for **2**

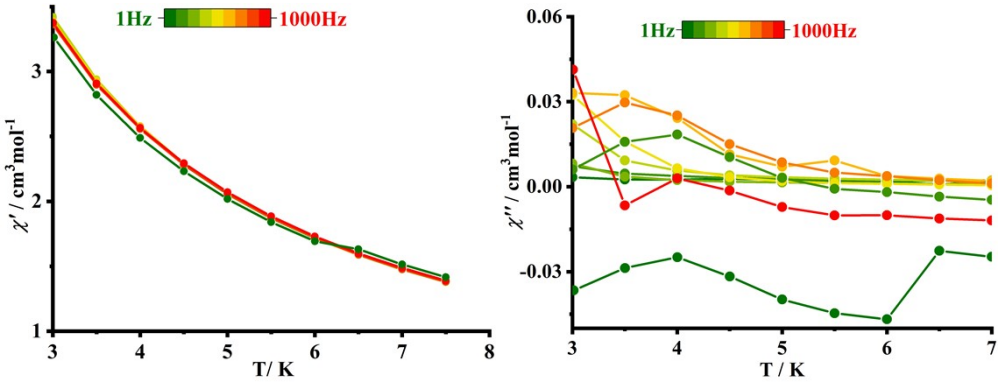

Fig. S10 Temperature dependence of the in-phase (χ') ac susceptibility (left) and the out-of-phase (χ'') ac susceptibility (right) in the temperature range 3-7 K of **1** under 0 Oe.

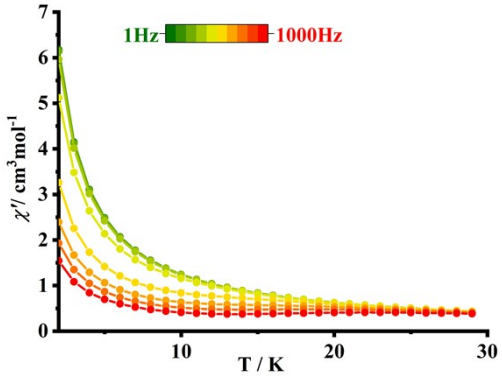

Fig. S11 Temperature dependence of the in-phase (χ') ac susceptibility in the temperature range 2-29 K of complex **2** under 0 Oe.

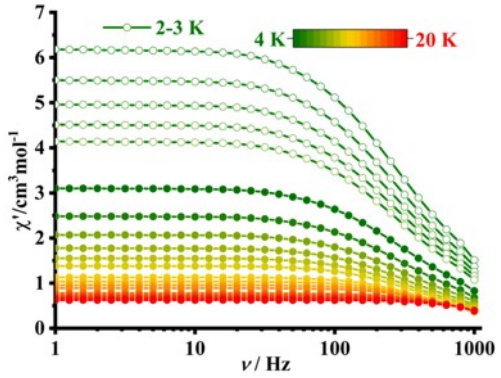

Fig. S12 Frequency dependence of the in-phase (χ') ac susceptibility in the temperature range 2-20 K of complex **2** under 0 Oe.

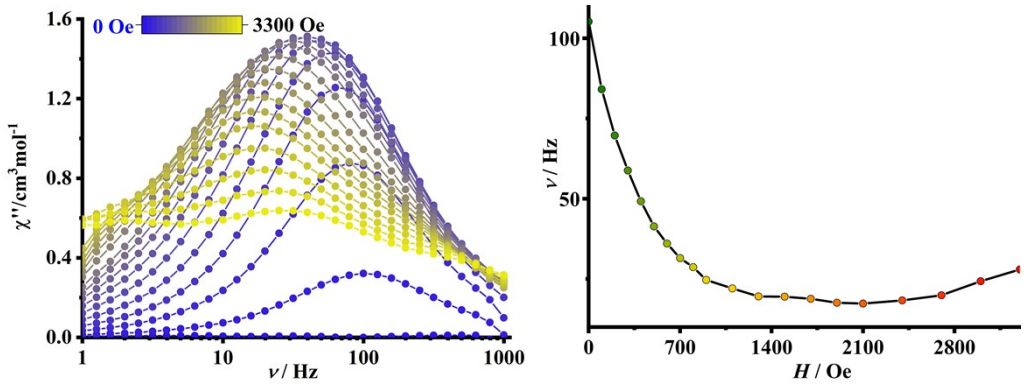

Fig. S13 Plot of the frequency dependence of the out-of-phase (χ'') ac susceptibility component under indicated dc field at 3 K for complex **1** (left). Plot of 1/τ vs. H for **1** under different dc fields at 3 K (right), the solidline is guide for eyes.

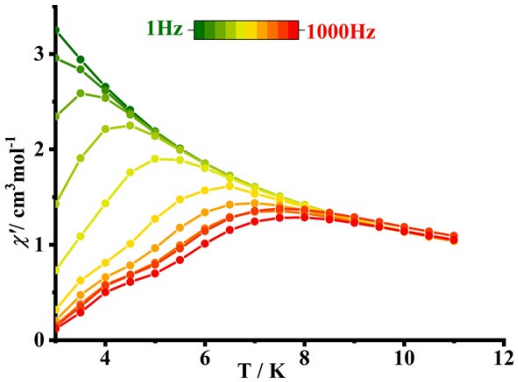

Fig. S14 Temperature dependence of the in-phase (χ') ac susceptibility in the temperature range 3-11 K of complex **1** under 2100 Oe.

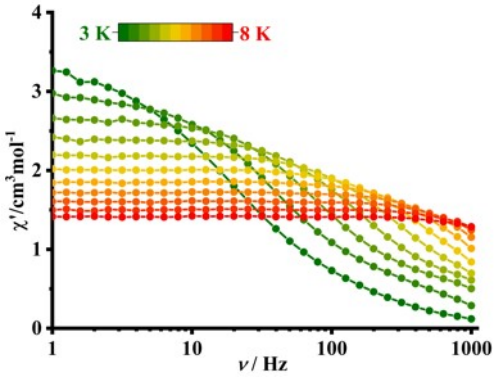

Fig. S15 Frequency dependence of the in-phase (χ') ac susceptibility in the temperature range 3-8 K of complex **1** under 2100 Oe.

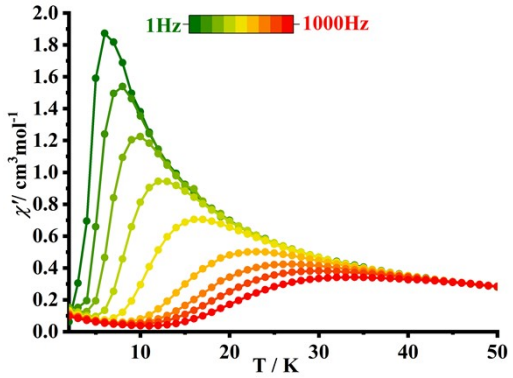

Fig. S16 Temperature dependence of the in-phase (χ') ac susceptibility in the temperature range 2-50 K of complex **2** under 1500 Oe.

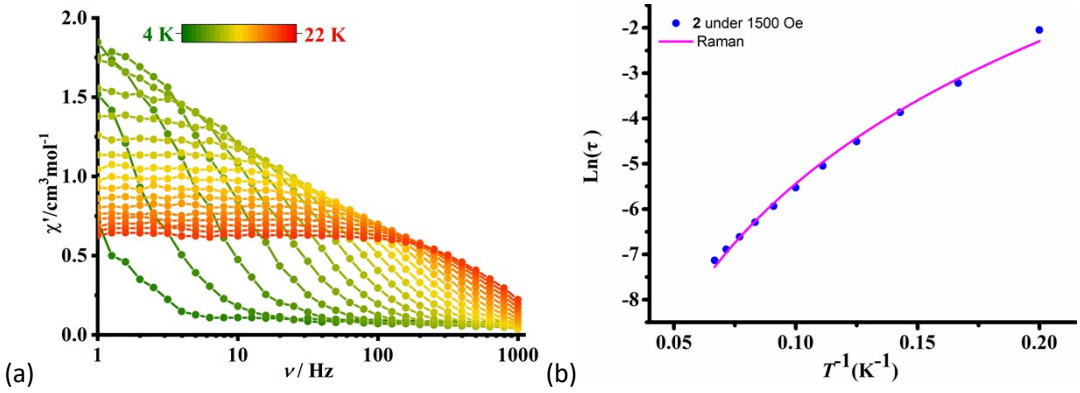

Fig. S17 (a) Frequency dependence of the in-phase (χ') ac susceptibility in the temperature range 2-22 K of complex **2** under 1500 Oe and (b) Ln(τ) curves of 1/*T* of **2** under 1500 Oe, the pink line represents the fitting of frequency-dependent data (at 5K - 15 K) by Raman mechanism.

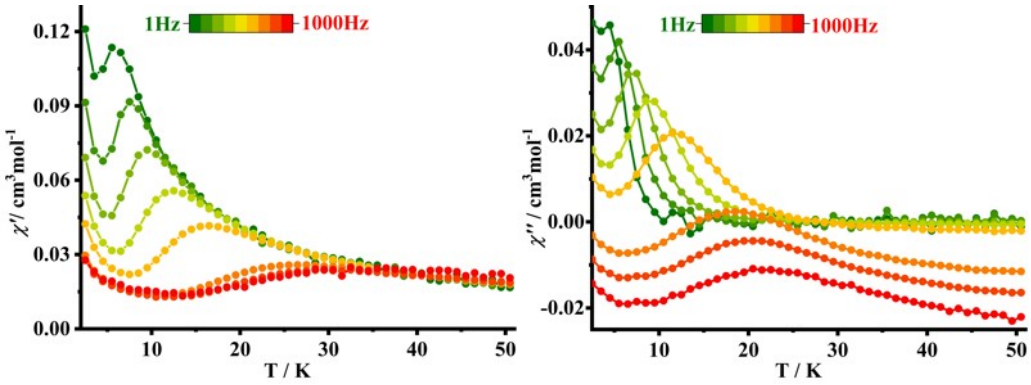

Fig. S18 Temperature dependence of the in-phase (χ') ac susceptibility (left) and the out-of-phase (χ'') ac susceptibility (right) in the temperature range 2.5-50.5 K of **2a** under 0 Oe.

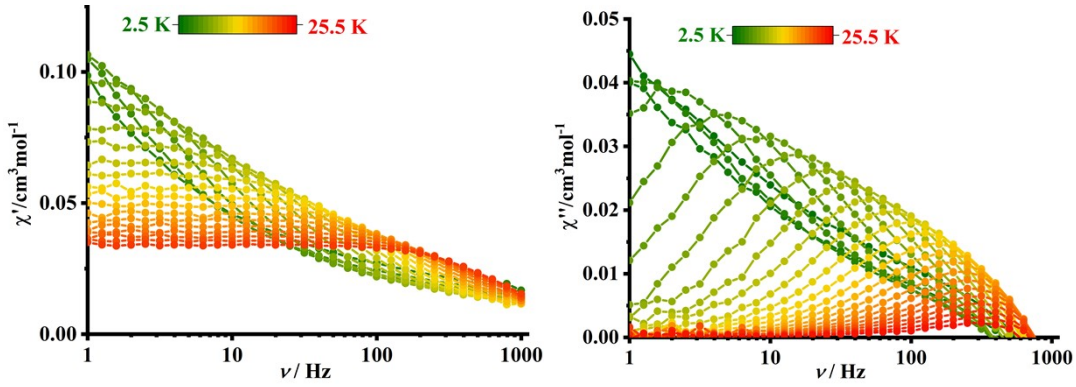

Fig. S19 Frequency dependence of the in-phase (χ') ac susceptibility (left) and the out-of-phase (χ'') ac susceptibility (right) in the temperature range 2.5-25.5 K of **2a** under 0 Oe.

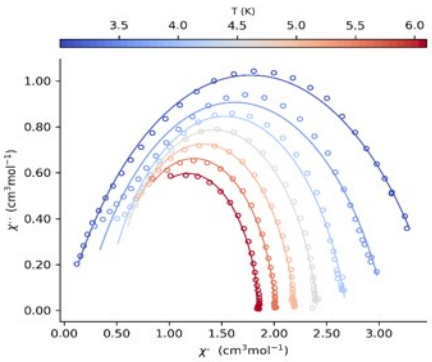

Fig. S20 Cole-Cole plots for **1** under 2100 Oe. The solid lines are the best fit for the generalized Debye model between 3.5 and 6 K.

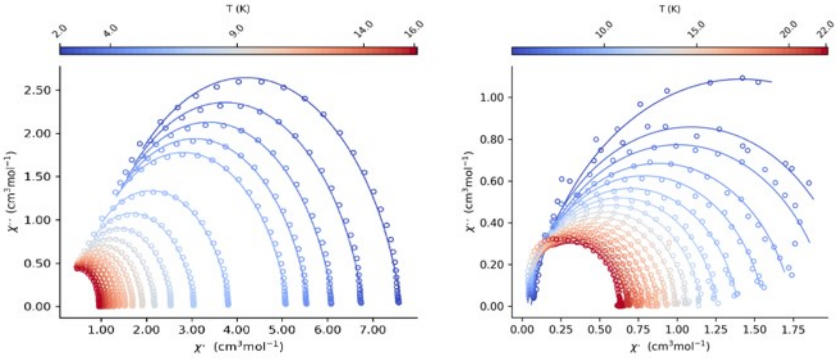

Fig. S21 Cole-Cole plots for **2** under 0 Oe (left, the best fit solid line between 2 and 15 k for the generalized Debye model) and 1500 Oe (right, the best fit solid line between 5 and 9 k).

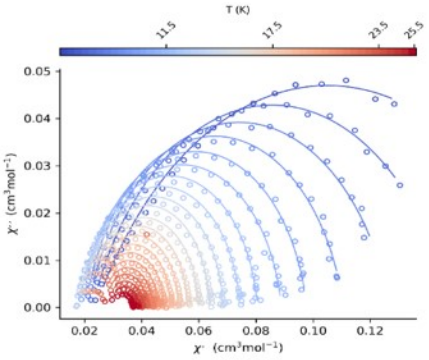

Fig. S22 Cole-Cole plots for **2a** under 0 Oe. The best fit solid line between 5.5 and 13.5 k for the generalized Debye model.

Table S6. Best fitted parameters (χ_T, χ_S, τ and α) with the extended Debye model for complex **1** at 2100 Oe in the temperature range 3-6 K, all τ values are used to fit in Fig. 4.

T/ K	χ_S / cm^3 mol^{-1}	χ_S error/ cm^3 mol^{-1}	χ_T / cm^3 mol^{-1}	χ_T error/ cm^3 mol^{-1}	τ/s	*τ error*/ s	α	α error
3	0.00099	0.00987	3.55036	0.0127	0.00770	8.37 E-5	0.33270	0.00416
3.5	0.18239	0.0227	3.06597	0.0178	0.00331	7.68 E-5	0.28490	0.00973
4	0.37529	0.0177	2.69040	0.00993	0.00174	3.13 E-5	0.19627	0.00855
4.5	0.43980	0.0115	2.41562	0.00461	0.00094	1.07 E-5	0.14325	0.00563
5	0.44651	0.00972	2.19804	0.00262	0.00053	5.01 E-6	0.11923	0.00437
5.5	0.45867	0.0100	2.01531	0.00176	0.00023	3.25 E-6	0.10222	0.00408
6	0.50471	0.0136	1.85685	0.00159	0.00021	3.21 E-6	0.07910	0.00519

Table S7. Best fitted parameters (χ_T, χ_S, τ and α) with the extended Debye model for complex **2** at 0 Oe in the temperature range 2-15 K, all τ values are used to fit in Fig. 4.

T/ K	χ_S / cm^3 mol^{-1}	χ_S error/ cm^3 mol^{-1}	χ_T / cm^3 mol^{-1}	χ_T error/ cm^3 mol^{-1}	τ/s	*τ error*/ s	α	α error

2	0.75940	0.0441	7.62999	0.01147	0.00537	6.33E-6	0.16477	0.000487
2.25	0.67501	0.0410	6.79308	0.01105	0.00528	6.48 E-6	0.16401	0.000507
2.5	0.60766	0.0383	6.13066	0.00097	0.00520	6.59 E-6	0.16378	0.000521
2.75	0.54976	0.0358	5.58054	0.00089	0.00512	6.64 E-6	0.16414	0.000530
3	0.49968	0.0336	5.11851	0.00083	0.00504	6.69 E-6	0.16438	0.000539
4	0.36978	0.0275	3.83625	0.00065	0.00479	6.87 E-6	0.16315	0.000575
5	0.28932	0.0235	3.06927	0.00053	0.00455	6.91 E-6	0.16129	0.000601
6	0.23197	0.0218	2.55919	0.00047	0.00430	7.15 E-6	0.15794	0.000651
7	0.19831	0.0189	2.19265	0.00039	0.00408	6.71 E-6	0.14816	0.000649
8	0.16696	0.0177	1.91815	0.00035	0.00380	6.51 E-6	0.13759	0.000675
9	0.14920	0.0151	1.70439	0.00028	0.00355	5.65 E-6	0.12231	0.000636
10	0.11911	0.0144	1.53408	0.00025	0.00322	5.25 E-6	0.11153	0.000644
11	0.10025	0.0134	1.39413	0.00021	0.00292	4.71 E-6	0.09831	0.000629
12	0.081592	0.0121	1.27745	0.00017	0.00263	4.02 E-6	0.08521	0.000585
13	0.058544	0.0119	1.17889	0.00015	0.00234	3.65 E-6	0.07557	0.000575
14	0.041128	0.0114	1.09455	0.00012	0.00209	3.25 E-6	0.06555	0.000551
15	0.026156	0.0111	1.02197	0.00011	0.00187	2.96 E-6	0.05581	0.000534

Table S8. Best fitted parameters (χ_T, χ_S, τ and α) with the extended Debye model for complex **2** at 1500 Oe in the temperature range 5-22 K, in which the τ values with α > 0.1 are used to fit in Fig. S17b.

T/ K	χ_S / cm^3 mol^{-1}	χ_S error/ cm^3 mol^{-}	χ_T / cm^3 mol^{-1}	χ_T error/ cm^3 mol^{-}	τ/s	*τ error*/ s	α	α error
5	5.71E-02	6.63E-03	2.77235	6.68E-02	1.29E-01	5.27E-03	1.39E-01	1.14E-02
6	3.35E-02	1.11E-02	2.14434	3.64E-02	4.00E-02	1.22E-03	1.30E-01	1.44E-02
7	2.41E-02	7.76E-03	1.98517	1.67E-02	2.10E-02	3.70E-04	1.49E-01	8.86E-03
8	1.59E-02	5.88E-03	1.74944	8.82E-03	1.10E-02	1.34E-04	1.49E-01	6.38E-03
9	1.12E-02	5.10E-03	1.56380	5.75E-03	6.41E-03	6.43E-05	1.37E-01	5.41E-03
10	4.05E-03	5.63E-03	1.39569	5.01E-03	3.98E-03	4.34E-05	1.32E-01	5.93E-03
11	5.29E-22	5.61E-03	1.26270	4.07E-03	2.64E-03	2.83E-05	1.23E-01	5.89E-03
12	1.12E-24	6.24E-03	1.15799	3.77E-03	1.85E-03	2.18E-05	1.13E-01	6.52E-03
13	3.63E-19	7.43E-03	1.06857	3.79E-03	1.34E-03	1.89E-05	1.06E-01	7.71E-03
14	1.68E-15	7.45E-03	9.97436	3.23E-03	1.02E-03	1.42E-05	1.00E-01	7.62E-03

15	4.24E-14	2.97E-02	9.35438	1.13E-02	7.99E-04	4.51E-05	1.01E-01	2.99E-02
16	1.05E-16	1.36E-02	8.72565	4.35E-03	6.30E-04	1.63E-05	8.58E-02	1.36E-02
17	2.05E-22	1.19E-02	8.22411	3.37E-03	5.12E-04	1.17E-05	7.74E-02	1.17E-02
18	1.22E-21	1.14E-02	7.71907	2.75E-03	4.20E-04	9.25E-06	6.25E-02	1.10E-02
19	1.64E-16	1.55E-02	7.34987	3.24E-03	3.55E-04	1.09E-05	5.94E-02	1.46E-02
20	9.94E-22	1.45E-02	6.92973	2.84E-03	3.00E-04	8.70E-06	4.16E-02	1.36E-02
21	9.34E-23	1.69E-02	6.67605	2.63E-03	2.63E-04	9.21E-06	4.19E-02	1.50E-02
22	5.56E-23	1.53E-02	6.31E-01	2.17E-03	2.28E-04	7.41E-06	2.66E-02	1.35E-02

Table S9. Best fitted parameters (χ_T, χ_S, τ and α) with the extended Debye model for complex **2a** at 0 Oe in the temperature range 5.5-25.5 K, in which the τ values with $\alpha < 0.1$ are used to fit in Figure 4 (5.5 K-21.5 K).

T/ K	χ_S / cm^3 mol^{-1}	χ_S error/ cm^3 mol^{-}	χ_T / cm^3 mol^{-1}	χ_T error/ cm^3 mol^{-}	τ/s	τ *error/* s	α	α error
5.5	0.02384	0.000497	0.18627	0.00280	0.08407	3.41 E-3	0.33223	0.00894
6.5	0.02272	0.000412	0.14879	0.00106	0.03431	6.03 E-4	0.24002	0.00708
7.5	0.02115	0.000399	0.12708	0.000623	0.01773	2.31 E-4	0.18905	0.00662
8.5	0.02049	0.000475	0.11068	0.000513	0.01014	1.42 E-4	0.13807	0.00792
9.5	0.01964	0.000529	0.09780	0.000465	0.00636	1.02 E-4	0.10698	0.00944
10.5	0.01898	0.000621	0.08894	0.000438	0.00433	8.13 E-5	0.09262	0.0111
11.5	0.01908	0.000731	0.08046	0.000468	0.00309	7.32 E-5	0.06121	0.0145
12.5	0.01928	0.000724	0.07434	0.000396	0.00232	5.53 E-5	0.04625	0.0147
13.5	0.01995	0.000770	0.06844	0.0365	0.00178	4.66 E-5	0.02140	0.0165
14.5	0.02047	0.000958	0.06366	0.000486	0.00145	5.18E-5	0.00064	0.0237
15.5	0.02122	0.000791	0.05986	0.000306	0.00118	3.52E-5	0.00911	0.0187
16.5	0.02156	0.000988	0.05605	0.000420	0.00100	4.18E-5	2.33E-17	0.0272
17.5	0.02241	0.00102	0.05298	0.000389	0.00087	4.09 E-5	4.91E-25	0.0299
18.5	0.02339	0.00109	0.05018	0.000362	0.00076	4.28 E-5	1.68E-17	0.0344
19.5	0.02449	0.00103	0.04771	0.000304	0.00069	4.16 E-5	6.19E-17	0.0357
20.5	0.02559	0.00106	0.04552	0.000291	0.00064	4.53 E-5	5.57E-18	0.0412
21.5	0.02662	0.000996	0.04356	0.000259	0.00060	4.67 E-5	2.04E-17	0.0442
22.5	0.02749	0.00246	0.04163	0.000610	0.00057	1.30 E-4	1.85E-16	0.0127
23.5	0.02864	0.000982	0.03990	0.000251	0.00057	6.56 E-5	3.12E-16	0.0644
24.5	0.02946	0.000913	0.03831	0.000232	0.00057	7.69 E-5	2.68E-15	0.0759

25.5	0.03096	0.000740	0.03708	0.000159	0.00062	9.75 E-5	1.22E-17	0.0824

Computational detail

Complete-active-space self-consistent field (CASSCF) calculations on individual Dy^{III} fragments for complexes **1** and **2** (see Figure S23 for the calculated complete structures of **1** and **2**) on the basis of single-crystal X-ray determined geometry have been carried out with the OpenMolcas[S1] program package.

The basis sets for all atoms are atomic natural orbitals from the OpenMolcas[S1] ANO-RCC library: ANO-RCC-VTZP for Dy^{III}; VTZ for close N and O atoms; VDZ for distant atoms. The calculations employed the second order Douglas-Kroll-Hess Hamiltonian, where scalar relativistic contractions were taken into account in the basis set and the spin-orbit couplings were handled separately in the restricted active space state interaction (RASSI-SO) procedure.[S2–S3] Active electrons in 7 active orbitals include all *f* electrons (CAS (9 in 7) in the CASSCF calculation. To exclude all the doubts, we calculated all the roots in the active space. We have mixed the maximum number of spin-free state which was possible with our hardware (all from 21 sextets, 128 from 224 quadruplets, 130 from 490 doublets for Dy^{III}. SINGLE_ANISO[S2] program was used to obtain the energy levels, ***g*** tensors, magnetic axes, *et al.* based on the above CASSCF/RASSI-SO calculations.

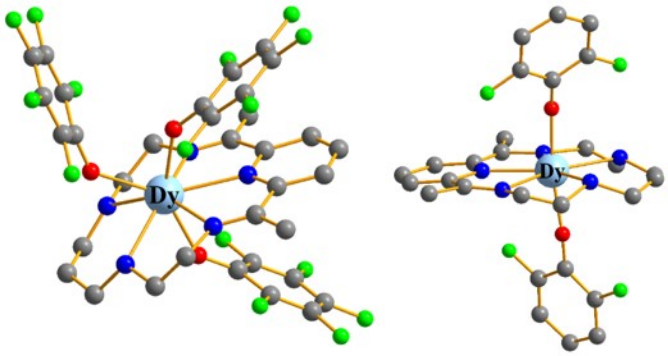

1 **2**

Fig. S23. Calculated complete structures of complexes **1** and **2**; H atoms are omitted for clarify.

Table S10. Calculated energy levels (cm^{-1}), ***g*** (g_x, g_y, g_z) tensors and predominant m_J values of the lowest eight Kramers doublets (KDs) of individual Dy^{III} fragments for complexes **1** and **2** using CASSCF/RASSI-SO with the OpenMolcas.

KDs	**1**			**2**		
	E	***g***	m_J	*E*	***g***	m_J
1	0.0	0.008 0.031 19.266	±15/2	0.0	0.004 0.006 19.852	±15/2

2	118.6	0.481 0.645 15.458	±13/2	368.7	0.116 0.329 16.746	±13/2
3	205.5	3.902 5.159 10.114		490.9	0.441 0.978 18.051	
4	279.3	7.722 5.591 0.434		527.1	2.188 3.656 12.421	
5	328.6	2.346 3.265 14.652		602.8	0.689 4.598 10.585	
6	392.9	0.560 1.096 15.026		626.3	0.065 2.642 9.089	
7	531.9	0.071 0.218 17.832		709.8	1.010 3.203 8.220	
8	543.4	0.052 0.246 18.976		760.6	1.430 6.206 13.814	

Table S11. Wave functions with definite projection of the total moment | m_J > for the lowest eight KDs of individual Dy^{III} fragments for complexes **1** and **2**.

	E/cm^{-1}	wave functions
1	0.0	90.6%|±15/2>
	118.6	72.6%|±13/2>+20.4%|±9/2>
	205.5	44.2%|±11/2>+33.6%|±7/2>+5.8%|±1/2>+5.2%|±5/2>+3.9%|±13/2>
	279.3	39.8%|±5/2>+31.5%|±9/2>+11.1%|±11/2>+7.9%|±13/2>
	328.6	43.6%|±3/2>+23.3%|±1/2>+15.5%|±7/2>+6.8%|±5/2>+4.7%|±11/2>
	392.9	38.7%|±1/2>+14.0%|±9/2>+11.6%|±11/2>+11.3%|±7/2>+10.1%|±31/2>+7.4 %|±5/2>
	531.9	24.2%|±5/2>+23.7%|±7/2>+17.9%|±9/2>+15.7%|±3/2>+10.2%|±11/2>
	543.4	24.7%|±1/2>+19.7%|±3/2>+16%|±5/2>+14.4%|±7/2>+12.5%|±9/2>+8.7%|±1 1/2>
2	0.0	99.8%|±15/2>
	368.7	91.9%|±13/2>
	490.9	60.1%|±1/2>+23.8%|±3/2>+9.2%|±5/2>
	527.1	31.5%|±3/2>+27.1%|±11/2>+15.8%|±11/2>+8.8%|±7/2>+8.2%|±1/2>
	602.8	31.0%|±5/2>+21.3%|±11/2>+15.5%|±7/2>+14.9%|±3/2>+8.7%|±1/2>
	626.3	26.6%|±5/2>+23.7%|±11/2>+16.5%|±3/2>+13.6%|±7/2>+10.1%|±1/2>
	709.8	32.2%|±7/2>+26.8%|±9/2>+16.8%|±11/2>+14.7%|±5/2>
	760.6	40.7%|±9/2>+27.5%|±7/2>+11.7%|±5/2>+9.4%|±3/2>+5.7%|±1/2

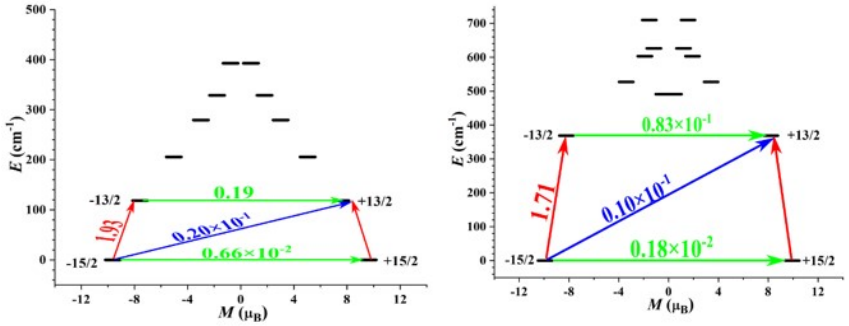

1 **2**

Fig. S24. Magnetization blocking barriers of individual Dy^{III} fragments for **1** and **2**. The thick black lines represent the KDs as a function of their magnetic moment along the magnetic axis. The green lines correspond to diagonal quantum tunneling of magnetization (QTM); the blue lines represent off-diagonal relaxation process. The numbers at each arrow stand for the mean absolute value of the corresponding matrix element of transition magnetic moment.

Table S12. Calculated the crystal-field parameters *B* (*k, q*) and corresponding weight for compounds **1** and **2** using CASSCF/RASSI-SO with the OpenMolcas.

1				**2**			
k	*q*	*B* (*k*, *q*)	Weight (%)	*k*	*q*	*B* (*k*, *q*)	Weight (%)
2	–2	0.1074×10^{1}	2.73	2	–2	0.2219×10^{1}	5.57
	–1	0.1117	0.28		–1	-0.1750×10^{1}	4.39
	0	-0.4872×10^{1}	12.39		0	-0.6702×10^{1}	16.82
	1	–0.9409	2.39		1	0.1412×10^{1}	3.54
	2	-0.5917×10^{1}	15.06		2	0.7973	2.00
4	–4	-0.3752×10^{-2}	0.77	4	–4	-0.2373×10^{-1}	4.81
	–3	0.5343×10^{-2}	1.09		–3	0.6323×10^{-2}	1.28
	–2	0.1099×10^{-1}	2.26		–2	-0.8682×10^{-2}	1.76
	–1	-0.4924×10^{-2}	1.01		–1	0.6566×10^{-2}	1.33
	0	-0.1982×10^{-1}	4.07		0	-0.8872×10^{-1}	18.00
	1	0.2895×10^{-2}	0.59		1	-0.5523×10^{-2}	1.12
	2	-0.4562×10^{-1}	9.38		2	-0.3416×10^{-4}	0.01
	3	-0.1590×10^{-1}	3.27		3	-0.5046×10^{-2}	1.02
	4	0.2247×10^{-1}	4.62		4	-0.1144×10^{-1}	2.32
6	–6	-0.8272×10^{-4}	0.63	6	–6	-0.4243×10^{-3}	3.23
	–5	-0.1697×10^{-5}	0.01		–5	-0.8645×10^{-4}	0.65
	–4	-0.4029×10^{-3}	3.11		–4	-0.3665×10^{-3}	2.79
	–3	-0.9712×10^{-5}	0.07		–3	0.2099×10^{-3}	1.60
	–2	-0.9777×10^{-4}	0.75		–2	0.1429×10^{-3}	1.09
	–1	0.1198×10^{-3}	0.92		–1	0.6446×10^{-3}	4.91
	0	0.5127×10^{-4}	0.39		0	0.4509×10^{-5}	0.03
	1	-0.2949×10^{-3}	2.27		1	-0.4320×10^{-3}	3.29
	2	-0.2378×10^{-4}	0.18		2	-0.5159×10^{-4}	0.39
	3	-0.6374×10^{-3}	4.92		3	-0.9752×10^{-4}	0.74
	4	0.1368×10^{-2}	10.57		4	-0.2529×10^{-3}	1.92
	5	-0.1201×10^{-2}	9.28		5	-0.2503×10^{-3}	1.90
	6	0.5066×10^{-3}	3.91		6	0.1259×10^{-2}	9.60

Table S13. Calculate charge on oxygen atom of the respective phenolate ligands using LoProp population analysis.

Coordination Atoms	**1**	**2**
O1	-0.8473	-0.9239
O2	-0.8775	-0.9181
O3	-0.8456	---
Average charge density	-0.8568	-0.9210

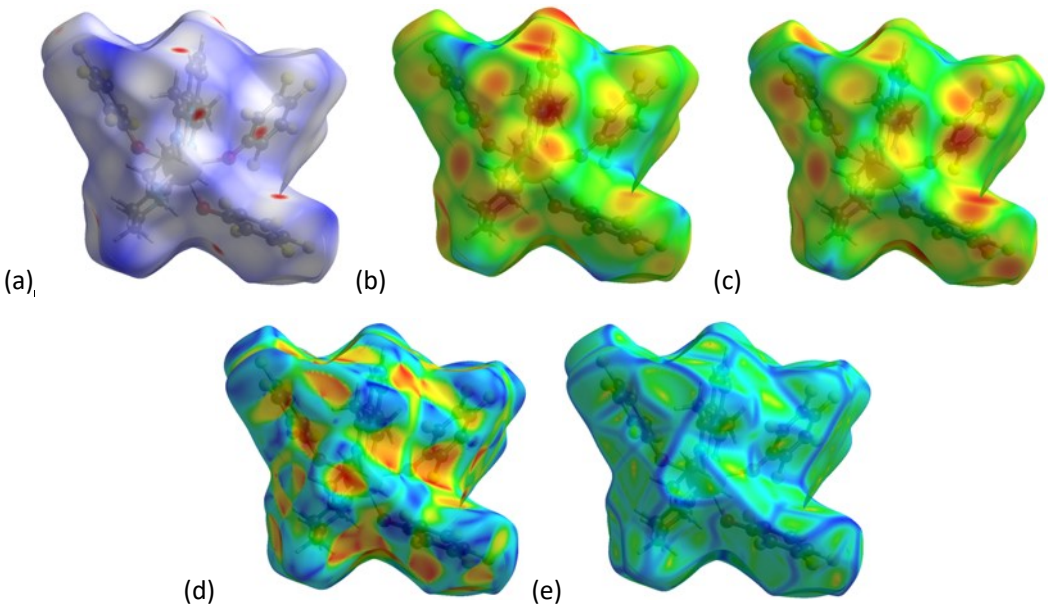

Fig. 25. An ensemble of HSs for the complex **1** molecule decorated with different properties available in *CrystalExplorer*. (a): d norm; (b): di; (c): de; (d): Shape-index; (e): Curvedness.

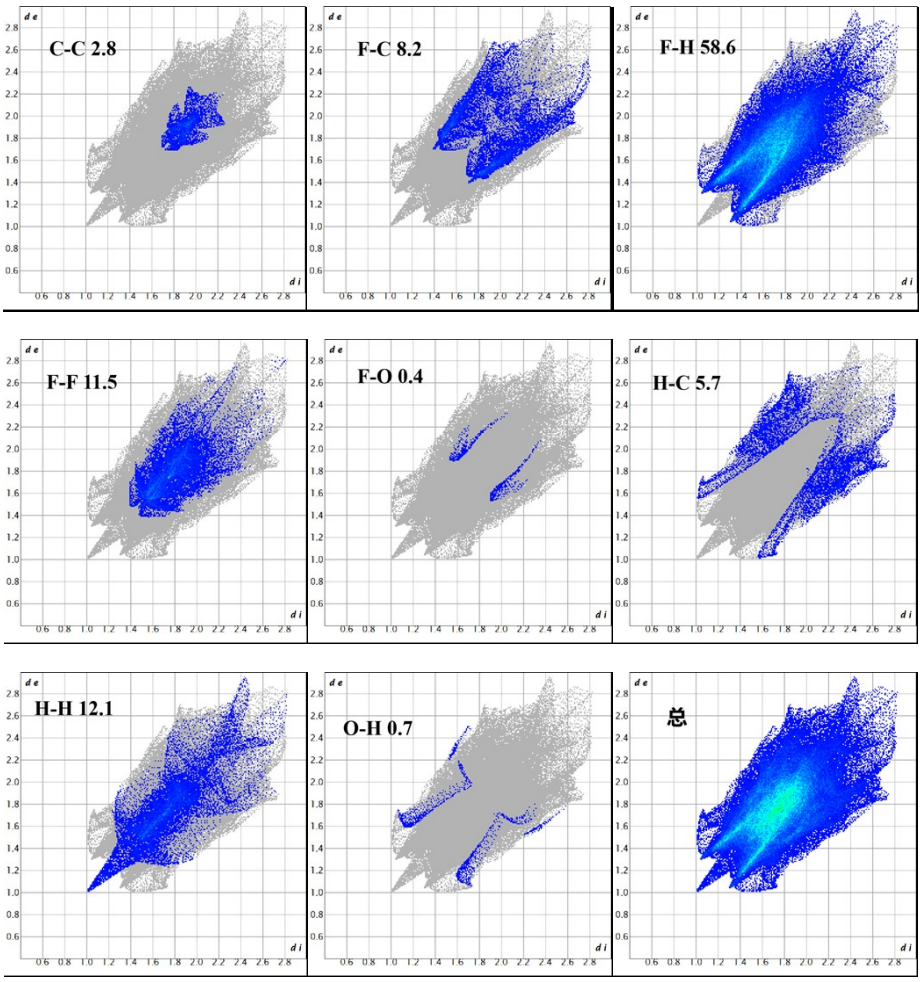

Fig. 26. The corresponding fingerprint plot for Complex **1**

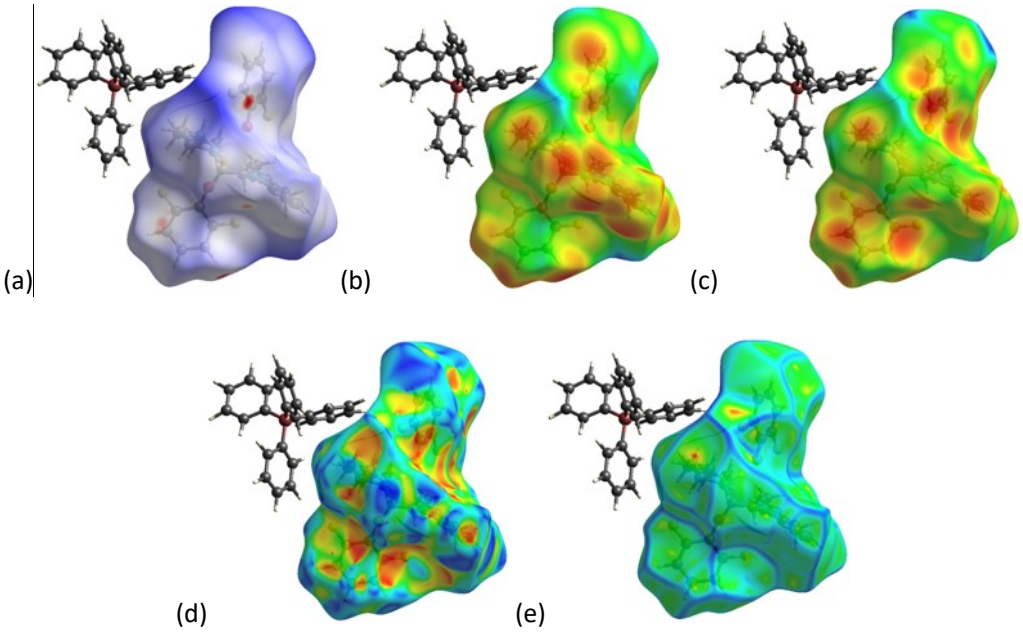

Fig. 27. An ensemble of HSs for the complex **2** molecule decorated with different properties available in *CrystalExplorer*. (a): d norm; (b): di; (c): de; (d): Shape-index; (e): Curvedness.

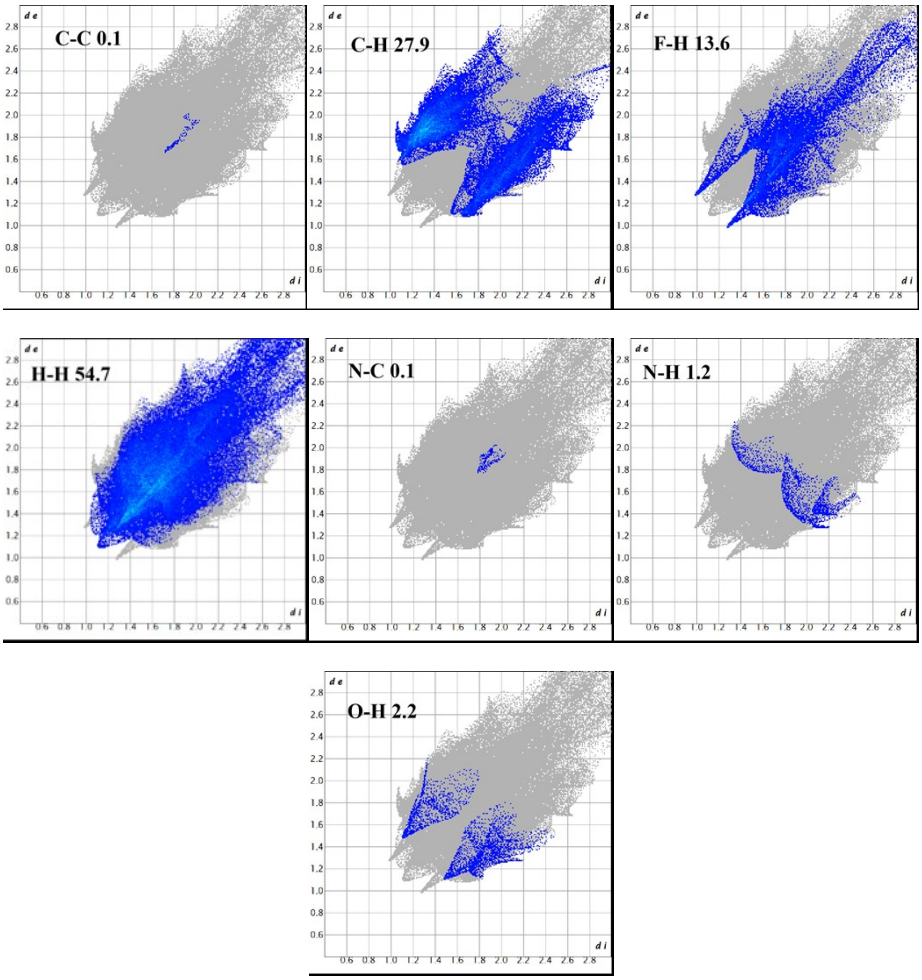

Fig. 28. The corresponding fingerprint plot for Complex **2**

References:

S1 Galván, I. F.; Vacher, M.; Alavi, A.; Angeli, C.; Aquilante, F.; Autschbach, J.; Bao, J. J.; Bokarev, S. I.; Bogdanov, N. A.; Carlson, R. K.; Chibotaru, L. F.; Creutzberg, J.; Dattani, N.; Delcey, M. G.; Dong, S. S.; Dreuw, A.; Freitag, L.; Frutos, L. M.; Gagliardi, L.; Gendron, F.; Giussani, A.; González, L.; Grell, G.; Guo, M. Y.; Hoyer, C. E.; Johansson, M.; Keller, S.; Knecht, S.; Kovacevic, G.; Källman, E.; Manni, G. L.; Lundberg, M.; Ma, Y. J.; Mai, S.; Malhado, J. P.; Malmqvist, P. Å.; Marquetand, P.; Mewes, S. A.; Norell, J.; Olivucci, M.; Oppel, M.; Phung, Q. M.; Pierloot, K.; Plasser, F.; Reiher, M.; Sand, A. M.; Schapiro, I.; Sharma, P.; Stein, C. J.; Sørensen, L. K.; Truhlar, D. G.; Ugandi, M.; Ungur, L.; Valentini, A.; Vancoillie, S.; Veryazov, V.; Weser, O.; Wesołowski, T. A.; Widmark, P.; Wouters, S.; Zech, A.; Zobel, J. P.; Lindh. R. *J. Chem. Theory Comput.* **2019**, *15*, 5925–5964.

S2 Malmqvist, P. Å.; Roos, B. O.; Schimmelpfennig, B. *Chem. Phys. Lett.,* **2002**, *357,* 230–240.

S3 Heß, B. A.; Marian, C. M.; Wahlgren, U.; Gropen, O. *Chem. Phys. Lett.,* **1996**, *251,* 365–371.

S4 Chibotaru, L. F.; Ungur, L.; Soncini, A. *Angew. Chem., Int. Ed*. **2008**, *47*, 4126–4129.

S5 Ungur, L.; Van den Heuvel, W.; Chibotaru, L. F. *New J. Chem.* **2009**, *33*, 1224–1230.

S6 Chibotaru, L. F.; Ungur, L.; Aronica, C.; Elmoll, H.; Pilet, G.; Luneau, D. *J. Am. Chem. Soc*. **2008**, *130*, 12445–12455.

S7 Lines, M. E. *J. Chem. Phys*. **1971**, *55*, 2977−2984.

S8 Mondal, K. C.; Sundt, A.; Lan, Y. H.; Kostakis, G. E.; Waldmann, O.; Ungur, L.; Chibotaru, L. F.; Anson, C. E.; Powell, A. K. *Angew. Chem., Int. Ed.* **2012**, *51*, 7550−7554.

S9 Langley, S. K.; Wielechowski, D. P.; Vieru, V.; Chilton, N. F.; Moubaraki, B.; Abrahams, B. F.; Chibotaru, L. F.; Murray, K. S. *Angew. Chem., Int. Ed.* **2013**, *52*, 12014–12019.